Probabilistic Engineering Mechanics 77 (2024) 103642

Contents lists available at ScienceDirect

Probabilistic Engineering Mechanics

journal homepage: www.elsevier.com/locate/probengmech

Bayesian model updating of eight-storey CLT building using modal data

Blaž Kurent [a,*], Noemi Friedman [b], Angelo Aloisio [c], Dag Pasca [d], Roberto Tomasi [e], Boštjan Brank [a]

[a] Faculty of Civil and Geodetic Engineering, University of Ljubljana, Ljubljana, Slovenia
[b] Informatics Laboratory, Institute for Computer Science and Control (SZTAKI), Hungary
[c] Department of Civil, Construction-Architectural and Environmental Engineering, Università degli Studi dell'Aquila, L'Aquila, Italy
[d] Norsk Treteknisk Institutt (Norwegian Institute of Wood Technology), Oslo, Norway
[e] Faculty of Science and Technology, Norwegian University of Life Sciences, Ås, Norway

ARTICLE INFO

Keywords:
CLT building
Modal testing
Model updating
Bayesian inference
Surrogate model
Parametric study

ABSTRACT

The serviceability of tall timber buildings due to wind-induced vibrations is often a governing design criterion. However, accurate modelling of such buildings for their serviceability is a challenge, partly because certain non-structural building elements (e.g. plasterboards, façade, screed) act structurally, and no guidelines exist on how to effectively include them in the model. Model updating may be helpful in revealing their as-built characteristics. This paper presents findings of a surrogate-based Bayesian model updating of a lightweight eight-storey cross-laminated-timber building. In particular, the focus was on patterns and correlations between mass distribution and modal characteristics, as well as the effects of joints, non-structural building elements, and the foundation. Model updating utilised the results of ambient vibration testing, which is commonly used in civil engineering for structural identification or health monitoring, however, it generally offers a relatively low number of identified modes. To this end, the study investigates the sensitivity of the updating process to the number of modes involved in the analysis.

1. Introduction

Timber as a structural material is becoming increasingly popular, which has highlighted some unique challenges, particularly vibration issues due to its lightweight nature [1]. Additionally, developing high-rise timber buildings introduced complexities in managing wind-induced vibrations [2]. Research on the dynamic response of timber buildings started more than 20 years ago [3], focusing initially on experimental investigations [4–7]. Early studies primarily concentrated on timber-framed structures, which are prevalent in North America housing [8–11]. The growing use of cross-laminated timber (CLT) and engineered wood products, especially in seismic-prone areas [12], fuelled research on the dynamic characterisation of mass-timber buildings. The characterisation spanned from the dynamic identification of existing buildings or laboratory prototypes [13].

During the initial phase of research, spanning almost 20 years, timber engineering progress has been relatively slow compared to other engineering fields [14–17]. Initially, the main focus was on assessing modal parameters through operational modal analysis or forced vibration tests [18]. Notably, the extensive ambient vibration testing (AVT) database compiled by Reynolds et al. [5,19] and Feldmann et al. [4], represents a significant contribution in this field to date. In recent years, Abrahamsen et al. [2] performed dynamic tests within the DynaTTB research program to estimate damping for tall timber buildings. Larsson et al. [20] conducted AVT to identify dynamic properties during the construction of a nine-storey timber-concrete hybrid building. Furthermore, Medel-Vera [21] proposed predictive models for the fundamental period of vibration in CLT buildings for seismic design. Numerous studies in the past years have focused on numerical investigations involving various structural systems, such as post-and-beams, CLT, etc., through case studies and parametric analyses [22–30].

In the past decade, the application of model updating in the field of timber buildings has gained momentum, focusing on solving inverse problems where modal parameters are utilised to assess model parameters. The evolution of model-updating applications in this field has followed a similar trend observed in related disciplines. Initially, early attempts relied on manual adjustment and hand-tuning for model updating [31,32], where optimal parameters were determined through a trial-and-error process. Subsequently, the proliferation of application

* Corresponding author.
E-mail address: bkurent@fgg.uni-lj.si (B. Kurent).

https://doi.org/10.1016/j.probengmech.2024.103642
Received 2 November 2023; Received in revised form 4 March 2024; Accepted 6 June 2024
Available online 8 June 2024

user interfaces in commercial finite element software facilitated the adoption of more rigorous model updating practices based on deterministic or probabilistic approaches [33,34]. Deterministic approaches emerged first and have witnessed numerous applications in the last five years [35–38].

However, deterministic model updating has certain limitations compared to probabilistic model updating. In general, deterministic model updating cannot quantify uncertainty, consider measurement errors, comprehensively explore the parameter space, account for model-form uncertainty, and incorporate prior information [39,40]. Specifically, deterministic model updating assumes fixed and deterministic updated model parameters without providing a direct measure of uncertainty. Conversely, it assumes error-free observed data, possibly leading to biased or inaccurate model updates. The limited exploration of parameter space leads to estimating a single set of updated model parameters that best fit the observed data, potentially overlooking alternative parameter combinations. Notably, it also neglects epistemic uncertainty, as it assumes a known and fixed mathematical form for the model, and does not incorporate prior knowledge about parameter values.

Probabilistic model updating offers a robust framework for addressing the limitations mentioned in deterministic model updating within structural engineering. Although there are numerous advantages to using probabilistic model updating, its application to timber buildings is relatively limited. For instance, Leyder et al. [41] and Kurent et al. [42] presented Bayesian updating approaches for timber structures. Leyder et al. conducted a sensitivity analysis to identify critical model parameters and then estimated the posterior distribution of these parameters using the BASIS implementation. In related work, Kurent et al. extended their previous study [36] by developing a surrogate-based Bayesian update of the model parameters. Bezabeh et al. [43,44] proposed a probabilistic procedure to evaluate the serviceability performance of tall mass-timber buildings. Considering uncertainty in timber engineering is crucial, necessitating the estimation of model parameters and their relative uncertainties.

Additional research on Bayesian model updating of timber buildings is highly desirable as it has the potential to provide crucial uncertainty bounds for the model parameters in timber engineering. This would enhance the understanding of the inherent variability and uncertainties associated with timber structures, thereby enabling more accurate and reliable assessments of their behaviour. It must be remarked that when performing model updating using AVT, it is crucial to assume either the mass or stiffness to have a well-posed inverse problem. Existing literature has not adequately explored how mass uncertainty affects modal properties. Furthermore, the effect of secondary elements, often overlooked in model updating, is especially important in lightweight structures.

This study focuses on the Bayesian model updating of an eight-storey CLT structure in Ås, Norway. Previous research by Aloisio et al. [35] and Ussher et al. [45] have investigated this building, but their attempts focused on deterministic model updating without considering uncertainty in the estimates. By applying Bayesian inference in the context of timber engineering, this study provides a better exploration of this case study and addresses gaps in the existing literature. Specifically, the research aims to identify patterns and correlations between mass distribution and modal characteristics, offering practical structural design and optimisation insights. Additionally, the study will consider the effect of secondary elements on the outcomes of model updating, explicitly examining the impact of parapets and lintels on the dynamic behaviour of timber structures.

The study aims to characterise the sensitivity of the updating process to the number of modes involved in the analysis, since, to the authors' knowledge, previous research did not explicitly examine the relationship between the number of modes and the accuracy of the updated model. The Bayesian model updating will lead to identifying the as-built stiffness properties of the building with inherent uncertainties. Given the scarcity of examples of mid-rise buildings made entirely of wood, as most tested timber buildings are hybrid [46–49], the chosen case study serves as a valuable example of a fully CLT structure and has the potential to become a benchmark case study due to the significant interest it has generated from its investigation [45]. The data used in this paper will be made available for further research extensions.

2. Building description

The case study is an eight-storey student residential building, located in Ås, Norway. It has a total height of 27 m (which does not include one level of reinforced concrete basement). The rectangular plan measures 23 m × 15 m, as shown in Fig. 1a. Its load-bearing structure, including the room-separating walls and lift shaft, consists of CLT panels. The typical layout of the floors is shown in Fig. 1b. In each storey, there are nine prefabricated bathroom pods (denoted as toilets in the figure).

The building features large monolithic walls with high length-to-height ratios, assembled using tie-downs, angle brackets, and self-tapping screws. Under the room-separating walls, a 10 mm soundproofing resilient strip is installed. The external wall/floor/wall joint does not feature the resilient strip. A typical cross-section of an external wall/floor/wall joint is shown in Fig. 1c. The façade consists of 20 mm thick timber board cladding (see Fig. 1d) that is installed on 200 mm thick timber battens. On the indoor side, as shown in the illustrated cross-section, a 25 mm plasterboard covers the walls, however, some indoor walls remain exposed. Floor slabs are covered with oriented strand boards (OSB), which is a lightweight alternative for concrete screed. They are installed on the impact sound insulation layer, and topped with floor covering. The CLT panels that are used are manufactured by Mayr-Melnhof. The majority are 5-layer panels, with the exception of room-separating walls, which are 90 mm thick 3-layer panels. The rest of the walls have thicknesses from 100 mm to 180 mm and slabs between 180 mm and 220 mm. The building uses approximately 900 m^3 of timber for load-bearing structure, which means roughly 0.1 m^3 for each m^3 of building's volume.

3. Experiments

The AVT was performed in August 2022 under dry and clear weather conditions with moderate winds. The nearby weather station recorded a temperature of 26 °C and an average wind speed of 4 m/s at the time of the measurements, with gusts of up to 9 m/s. The building was in operation at the time of the experiments. The dynamic response was measured in three locations on the roof as shown in Fig. 2a. In each, three uniaxial sensors were used to measure accelerations in three orthogonal directions (see Fig. 2b). However, due to the low signal-to-noise ratio of accelerations in z direction, those signals were discarded. For the sensors, seismic ceramic shear piezoelectric accelerometers (PCB model 393B12) were used. The sensors have a sensitivity of approximately 10 V/g, a frequency range spanning from 0.15 to 1000 Hz, and a measurement range of up to approximately ±5 m/s^2. The accelerometers were connected to an HBM QuantumX data acquisition unit (24-bit analogue-to-digital converter) from Hottinger Brüel & Kjaer. Shielded polyurethane coaxial cables were used to ensure accurate and reliable data transmission. Two measurements, each lasting 90 min, were carried out. The data was sampled at a rate of 200 Hz, resulting in a total of 1,080,000 data points. The data was then downsampled applying first an anti-aliasing filter and then decimating the signal. Modal identification with SSIcov algorithm [50] available through the pyOMA python module [51] was used to identify four modes of vibration. The natural frequencies identified from analysing each of the two 90 min intervals are presented in Table 1. A stabilisation diagram of one of the two 90 min intervals is shown in Fig. 2c,

To explore the uncertainty of the experiments, both 90 min signals were windowed with a window length of 9 min and 75 % overlap, obtaining 80 intervals. Similarly to the case of the 90 min signal, SSicov

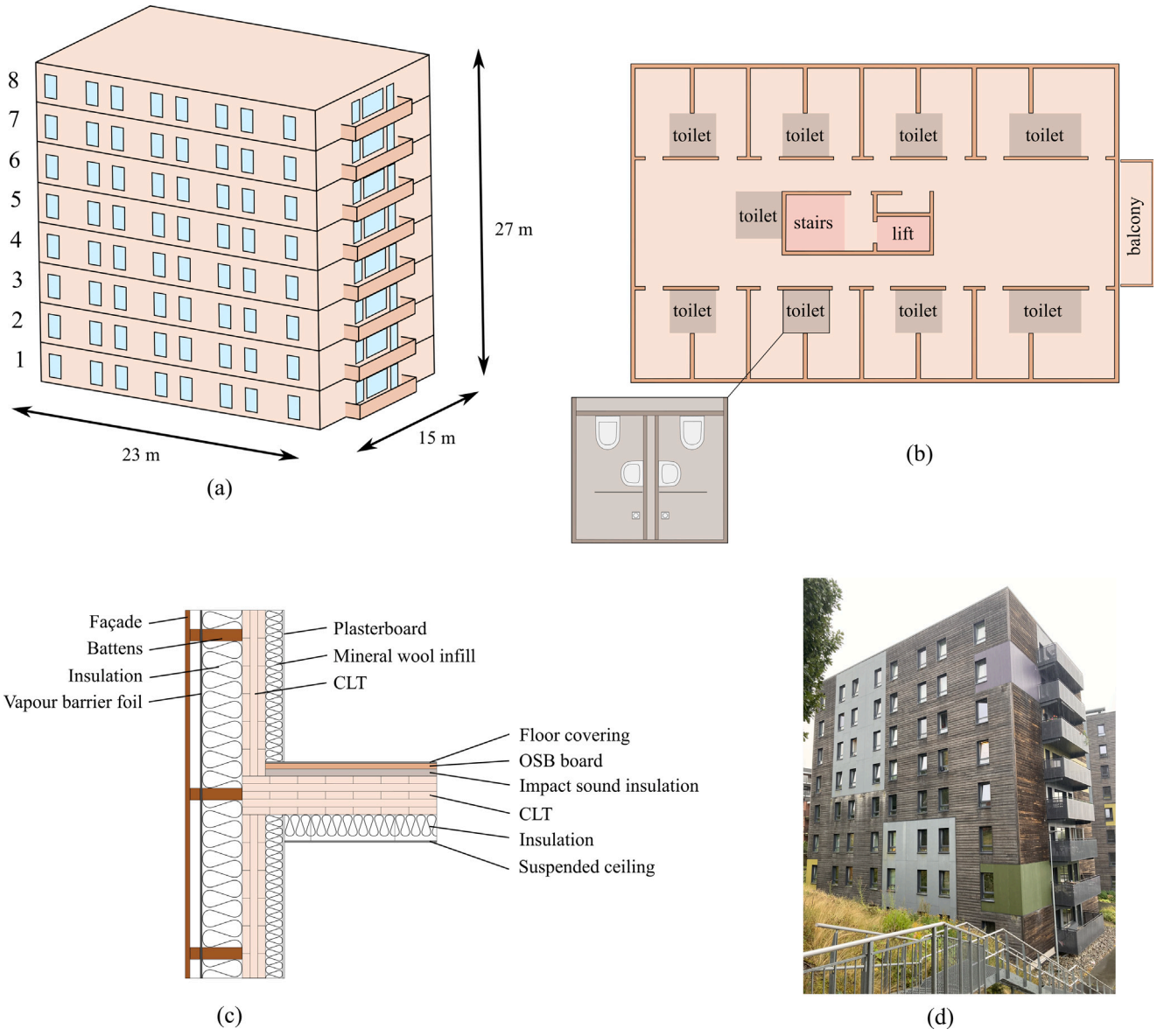

Fig. 1. General information about the building: (a) dimensions, (b) a typical layout, (c) a typical cross-section, and (d) a photo from August 2022.

modal identification was conducted on each 9 min interval to obtain four modes of vibration. A typical stabilisation diagram for a 9 min interval is shown in Fig. 2d. Altogether, 80 sets of modal properties are obtained from the windowed signal. The mean natural frequencies and corresponding coefficients of variation (COV) are displayed in Table 1 and their distributions are presented by histograms in Fig. 2e. They are approximated with a normal distribution (see blue lines in Fig. 2e) using mean frequencies and COV from Table 1. The mean mode shapes are visualised in Fig. 2f.

Table 1
Natural frequencies identified from modal analysis of 90 min and 9 min intervals.

Mode	90 min intervals		9 min intervals		
	1st interval	2nd interval	mean	st. deviation	COV
1	1.881 Hz	1.880 Hz	1.882 Hz	0.011 Hz	0.58 %
2	2.421 Hz	2.421 Hz	2.420 Hz	0.010 Hz	0.43 %
3	2.687 Hz	2.679 Hz	2.683 Hz	0.014 Hz	0.53 %
4	5.914 Hz	5.899 Hz	5.903 Hz	0.038 Hz	0.64 %

4. Numerical model

The initial FE model for computing natural frequencies and mode shapes was prepared in Ansys software. The assumptions, material properties and computed modal properties are described in Section 4.1. A parametric study evaluating some modelling assumptions is presented in Section 4.2 and a process of obtaining a surrogate model is shown in Section 4.3.

4.1. The initial model

The building is a complex system composed of a load-bearing structure and numerous non-structural components like façade, partition walls, plasterboards, windows, and stairs. In a timber building that weighs significantly less than an equivalent classical reinforced concrete building, such non-structural elements contribute to the modal properties and small amplitude dynamic response of the building, but

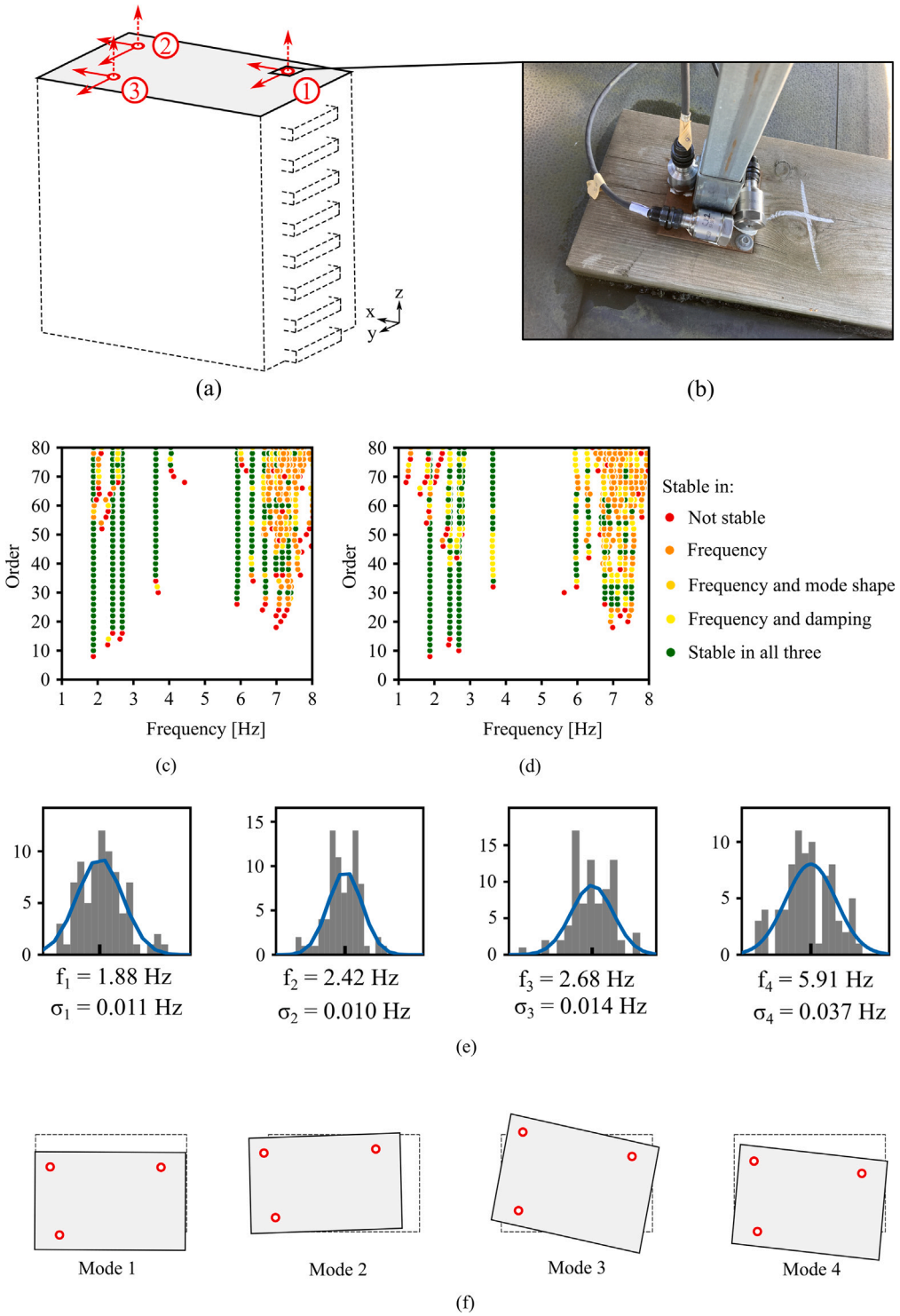

Fig. 2. AVT of an eight-storey CLT building: (a) layout of the sensor locations on the roof, (b) a photo of typical sensor location, (c) stabilisation diagram of the first 90 min interval, (d) stabilisation diagram of a typical 9 min interval, (e) histograms of the natural frequencies identified from the 80 windowed 9 min intervals (blue lines show estimation with normal distribution using mean and COV from Table 1), and (f) mode shapes identified from the first 90 min interval. (For interpretation of the references to colour in this figure legend, the reader is referred to the web version of this article.)

their contributions are hard to quantify. The model is simplified to the load-bearing structure, however, the influence of the neglected elements is explored with model updating in Section 5. Multi-layered shell elements (SHELL181 in Ansys) with an orthotropic material model for timber were used. The material properties that were assumed are taken from the European Technical Assessment (ETA) of the manufacturer and are shown in Table 2. The geometry was discretised by mesh with an approximate size of 0.3 m, which resulted in almost 92 thousand nodes.

The following modelling assumptions were adopted:

- Only the above-ground structure is modelled. One level of reinforced concrete basement is neglected.
- The foundation under the ground floor slab is assumed rigid.

Table 2
Material properties of timber according to the ETA of the manufacturer [52].

Material property	Value
Elastic modulus along the grain	$E_1 = 11\,600$ MPa
Elastic modulus perpendicular to the grain	$E_2 = 370$ MPa
In-plane shear modulus	$G_{12} = 250$ MPa
Transverse shear modulus	$G_{13} = 250$ MPa
Rolling shear modulus	$G_{23} = 50$ MPa

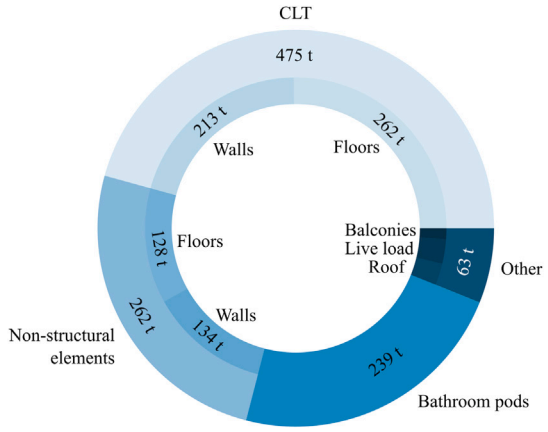

Fig. 3. Breakdown of the contributions to the total mass of the building.

- Connections between CLT panels are modelled as rigid.
- Floor slabs are modelled as deformable (i.e. the assumption of a rigid diaphragm is not made).
- The stairs are neglected.
- Windows and doors are neglected and modelled as openings.
- The stiffness of modular bathroom pods that are prefabricated and inserted in the CLT structure is neglected.
- Holes in floor slab smaller than 500 mm in diameter are neglected.
- Non-structural elements (plasterboards, façade, OSB boards, and similar) are neglected.
- The stiffness of the balconies is neglected.

Considering the mass of the building, elements that were neglected from the perspective of stiffness (non-structural elements, balconies, stairs, and modular bathroom pods) are included in the calculation. The breakdown of different contributions to the total mass of the building is Shown in Fig. 3. The majority of the mass is attributed to the CLT, non-structural elements (façade, insulation, plasterboard, OSB boards, suspended ceiling), and bathroom pods. Live load, balconies and the additional weight on the roof account for less than 10 %. The uncertainty of the weight estimation of the mass is high, which is largely contributed by poor documentation of bathroom pods. Typically, nine such modular pods are installed per each storey.

The weight of CLT panels is applied directly to the panels by assuming their density to be $\rho = 470\,\mathrm{kg/m^3}$. The weight of the non-structural elements is distributed over the panels on which they are attached. For instance, plasterboards, thermal insulation, and façade cladding are distributed over the CLT walls and OSB boards, floor covering, acoustic insulation, and suspended ceiling are distributed over the CLT floor slabs. Bathroom pods are distributed over the areas on the floor slabs where they are installed. The weight of the balconies is smeared over the external walls, and the live load which is estimated as $10\,\mathrm{kg/m^2}$ is distributed uniformly over the floor slabs. Additional weight on the roof is included to account for the ventilation and air conditioning installation. The total weight of the building is estimated at around 1.000 t, which, normalised to the building's volume, is approximately $110\,\mathrm{kg/m^3}$.

Table 3
Mass distribution simplification scenarios.

Scenario	Description of the scenario
Initial	Each CLT panel has an assigned mass based on its thickness. The mass of each non-structural element is distributed over the CLT panels to which it is attached. The mass of bathroom pods is distributed over the areas on the floor slabs where they are located.
M1	In each storey, the weight of the external walls with the attached non-structural elements is summed and uniformly distributed over the external walls. Separately, the weight of the internal walls is summed and smeared over the internal walls. The weight of the floor slabs with the attached non-structural elements and bathroom pods are uniformly distributed over the slabs.
M2	In each storey, the weight of all the walls with the attached non-structural elements is summed and uniformly distributed over them. The weight of the floor slabs is distributed as in M1.
M3	The weight of the floor slabs is distributed as in M1. The weight of all the walls with the attached non-structural elements in each storey is summed and distributed over the floor slabs. Half of the weight is distributed over the slab below and the rest over the slab above.
M4	The total weight of the building is distributed uniformly over all the walls and floors of the building.

The modal properties obtained by the initial FE model are shown in Fig. 4. The first two modes are bending in two main directions, the third mode is torsion, and the fourth mode is second-order bending in the weaker direction. The modal assurance criterion (MAC) matrix [53] is shown in Fig. 5a. A fairly good correlation can be observed in the diagonal terms, however, some level of spatial aliasing is recognised and is reflected in the high correlation between the first and the fourth modes. This may be easily justified by the placement of the sensors that is limited to the roof of the building, which cannot distinguish between the first-order bending and the second-order bending modes. Given that the two modes are well-separated in frequency, experimental modes can be easily matched with those of the FE model. The correlation of mode shapes is often presented with an FMAC plot [54], which is shown in Fig. 5b. The relative error of the ith natural frequency pair is calculated by

$$\mathrm{err}_{i,\mathrm{freq}} = \frac{f_{i,\mathrm{FE}} - f_{i,\mathrm{exp}}}{f_{i,\mathrm{exp}}}, \tag{1}$$

where $f_{i,\mathrm{FE}}$ and $f_{i,\mathrm{exp}}$ denote the natural frequencies obtained by the FE model and experiments, respectively.

4.2. Parametric study

In an attempt to shorten the modelling time, simplification of geometry or mass distribution might be made by the engineers. For this reason, several simplification scenarios have been tried to assess their effect on the natural frequencies. The simplification scenarios of mass distribution are described in Table 3 and the simplification scenarios regarding the modelling of geometry are presented in Table 4. In the case of mass simplification scenarios, the total mass of the building remains the same, while only its distribution changes. In the case of geometry simplification scenarios, the models differ in the way how the openings (windows and doors), parapets, and lintels are modelled.

See Figs. 6 and 7 for the effects of the mass and geometry simplifications, respectively. The assumptions of the initial model are the most accurate from the presented set of scenarios and therefore, its natural frequencies are taken as a reference. It may be observed that

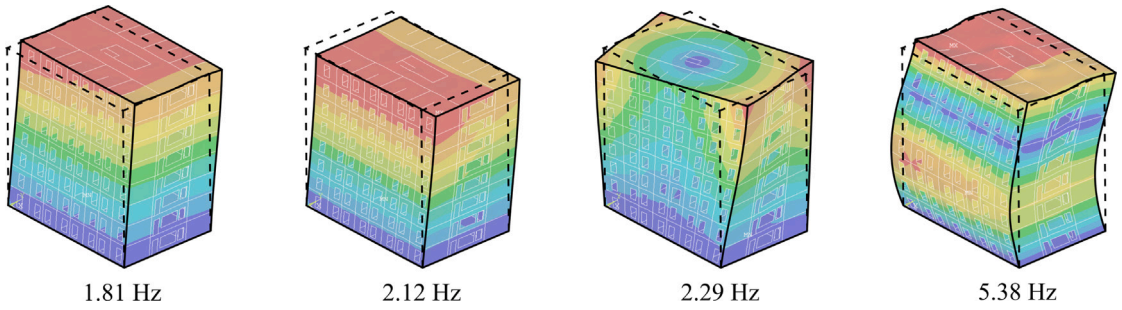

Fig. 4. Modes of vibration of the initial FE model.

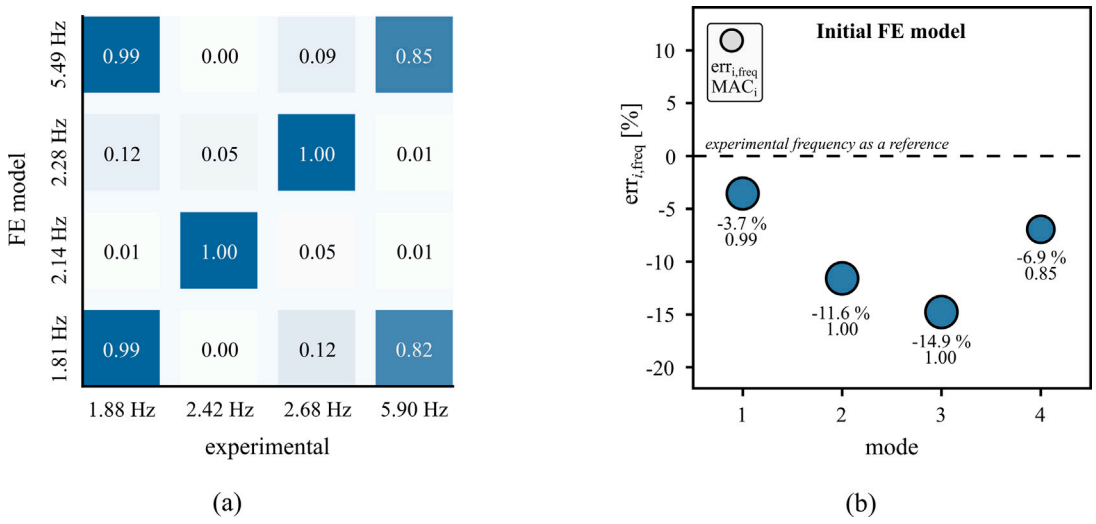

Fig. 5. Correlation of the experimental and FE modes presented by: (a) MAC matrix and (b) FMAC plot.

Table 4
Geometry simplification scenarios.

Scenario	Description of the scenario
Initial	All doors and windows are modelled as openings, while parapets and lintels are included in the model.
G1	All parapets below windows are neglected.
G2	All lintels above doors and windows are neglected.
G3	All lintels and parapets are neglected.
G4	Considering all windows on the external wall as filled, doors are left as openings
G5	Considering all openings (doors and windows) as filled.

by simplifying the distribution of the mass, the natural frequencies did not change significantly. Even when the total mass of the building was distributed over the whole building uniformly (scenario M4), the natural frequencies changed less than by 1.5 %. It should be noted, however, that no substantial mass imbalances were present in the design of the building. Any simplifications of mass distribution on other buildings should be considered carefully.

On the other hand, when the geometry of the building is simplified, natural frequencies are significantly influenced. Even as small simplification as neglecting parapets under the windows (scenario G1), reduces the first three natural frequencies up to 8.1 %. Therefore, it is suggested to be precise in the modelling of geometry.

4.3. Surrogate model

Stochastic analyses such as sensitivity analysis and Bayesian inversion are time-consuming, therefore, the surrogate model was made using generalised polynomial chaos (gPC) expansion. After the initial screening of the parameters through one-at-a-time sensitivity analysis, the five most important parameters were selected for model updating. They are defined in Table 5.

Let $\boldsymbol{P}$ be a random vector consisting of uncertain parameters $P_1, \dots, P_5$. For each realisation $\boldsymbol{p}$, modal properties can be computed by the FE model. The computation of the first four natural frequencies is denoted by forward operator $\mathcal{M}$, such that

$$\boldsymbol{f} = \left[f_1, f_2, f_3, f_4\right]^T = \mathcal{M}(\boldsymbol{p}). \tag{2}$$

The order of the natural frequencies $f_1, \dots, f_4$ is not defined by their increasing value, but rather by the mode they correspond to. What appears to be a simple task of ordering the modes can unravel into a complex problem [42] when $\mathcal{M}$ is deemed to be automatised. For now, the order of the modes is considered to be the same as that of the experimental modes. The procedure of the ordering is presented later in this section.

Besides the natural frequencies, the FE model computes their respective eigenvectors $\boldsymbol{\psi}_1, \dots, \boldsymbol{\psi}_4$ that are used for ordering the modes correctly. Namely, changing parameter values may change the order of the natural frequencies.

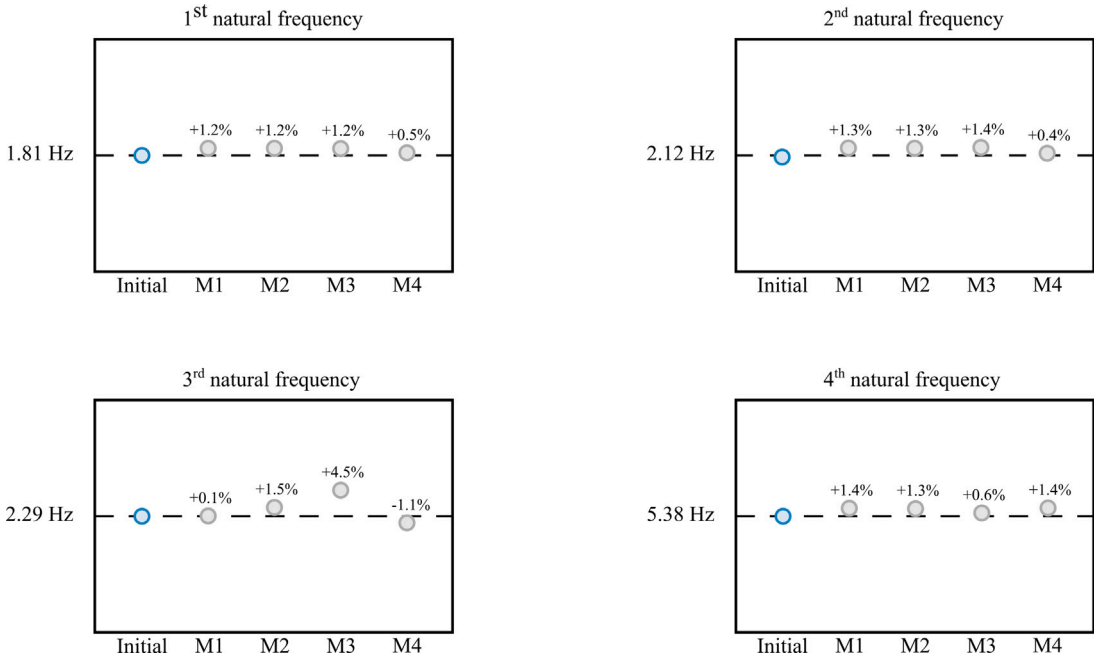

Fig. 6. The effect of different mass distribution assumptions on the natural frequencies. The initial model is taken as a reference.

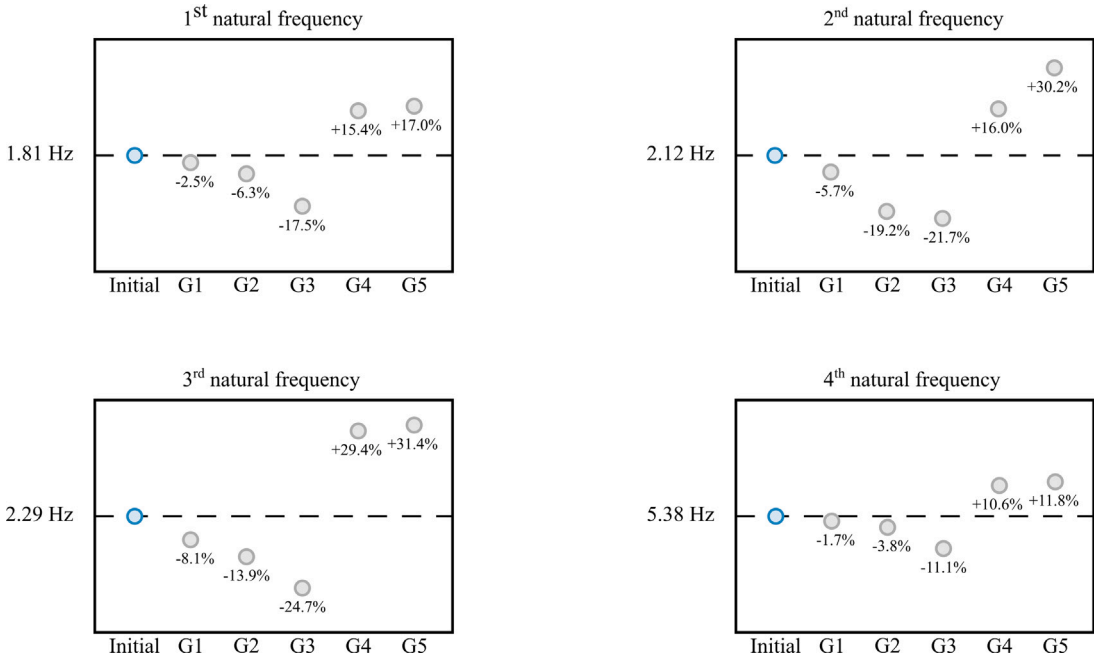

Fig. 7. The effect of different geometry modelling assumptions on the natural frequencies. The initial model is taken as a reference.

The FE model is replaced with a gPC-based surrogate model $\mathcal{M}_{\text{gPC}}$, that approximates the natural frequencies $\boldsymbol{f}_{\text{gPC}}$ in the form of multivariate polynomials of the input parameters

$$\boldsymbol{f} = \mathcal{M}(\boldsymbol{p}) \approx \boldsymbol{f}_{\text{gPC}} = \mathcal{M}_{\text{gPC}}(\boldsymbol{\theta}) = \sum_{m=1}^{M} \boldsymbol{\upsilon}_m \boldsymbol{\Phi}_m(\boldsymbol{\theta}), \tag{3}$$

where $\boldsymbol{\Phi}_m$ are the orthogonal multivariate polynomials and $\boldsymbol{\upsilon}_m \in \mathbb{R}^L$ are the coefficients of the expansion corresponding to the mth polynomial. For computational convenience, instead of directly using the random variables of the input parameter for the expansion, they are mapped to dimensionless reference random variables $\boldsymbol{\Theta} = [\Theta_1, \Theta_2, \Theta_3, \Theta_4, \Theta_5]^T$. The map from the reference parameters to the input parameters

$$\boldsymbol{p} = \mathcal{F}(\boldsymbol{\theta}) \tag{4}$$

is chosen such that the assumed uniform distribution is normalised to the $[-1, 1]$ interval for all of the random variables $\boldsymbol{\Theta}$. The joint distribution of random vector $\boldsymbol{\theta}$ may be computed as

$$\pi(\boldsymbol{\theta}) = \prod_{i=1}^{5} \pi(\theta_i) = \begin{cases} 0.5^5 & \text{for} \quad \boldsymbol{\theta} \in [-1, 1]^5 \\ 0 & \text{otherwise,} \end{cases} \tag{5}$$

assuming mutually independent random variables.

Table 5
Definition of the uncertain parameters to be calibrated.

Name	Range	Parameter definition
P_1	0.5–1.5	**Coefficient of vertical stiffness of the walls.** The reduction of the vertical stiffness is expected due to the effect of perpendicular-to-the-grain deformation of floor slabs under the walls in platform frame buildings [36]. The coefficient multiplies the elastic modulus along the fibres of the vertical layers of the wall panels, such that $E_{wall,vert} = P_1 \cdot E_1$.
P_2	1–3	**Coefficient of the in-plane shear stiffness of the walls.** The value of the in-plane shear modulus is highly uncertain. Considering academic literature on material properties of CLT [55], the value $G_{12} = 250$ MPa as provided in the ETA of the manufacturer might be largely underestimated. Namely, the in-plane shear modulus is observed to be between 450 MPa and 650 MPa, depending on whether the narrow sides of lamellae are glued or not. Furthermore, this coefficient includes a possible contribution of non-structural elements to the higher stiffness of the walls. The in-plane shear modulus of CLT walls is multiplied by this coefficient. Thus, the shear modulus of internal walls is defined as $G_{\text{walls,in}} = P_2 \cdot G_{12}$ (see row P_3 of this table for a definition of the shear modulus of the external walls).
P_3	1–1.5	**Coefficient of the in-plane shear stiffness of the external walls.** The coefficient accounts for the contribution of the façade to the higher stiffness of the external walls. Thus, the in-plane shear modulus of external walls is defined as $G_{\text{walls,ex}} = P_2 \cdot P_3 \cdot G_{12}$.
P_4	7–10	**The stiffness of the springs modelling the foundation.** A distributed spring under the ground floor slab is newly implemented (compared to the initial model that assumed a rigid foundation). Parameter P_4 defines its stiffness in the vertical direction, while the horizontal displacements of the ground floor remain constrained. A wide range of values is allowed, with the upper boundary being defined, such that the model behaves as a rigidly founded model. In order to include different orders of magnitude evenly, parameter P_4 is defined logarithmically, namely, the vertical spring stiffness is calculated as $k_{foundation} = 10^{P_4}$.
P_5	0.8–1.2	**Coefficient of the total mass of the building.** For all the elements of the building, upper and lower estimates of the mass were determined. The total mass of the building was thus estimated to be between the 80 % and 120 % of the initial estimate. Roughly half of the uncertainty is attributed to the uncertainty of bathroom pods, which are poorly documented. The coefficient P_5 is implemented as a multiplier of the total mass of the building.

The gPC expansion from (3) uses a set of M multivariate orthogonal polynomials $\{\boldsymbol{\Phi}_m\}_{m=1}^{M}$ for the approximation of $\boldsymbol{f}$. The orthogonality of the polynomials with respect to the underlying probability space is defined by

$$\begin{aligned}\mathbb{E}[\boldsymbol{\Phi}_m(\boldsymbol{\theta})\boldsymbol{\Phi}_n(\boldsymbol{\theta})] &= \int_{\mathbb{R}^N} \boldsymbol{\Phi}_m(\boldsymbol{\theta})\boldsymbol{\Phi}_n(\boldsymbol{\theta})\pi(\boldsymbol{\theta})\mathrm{d}\boldsymbol{\theta} \\ &= 0.5^5 \int_{[-1,1]^5} \boldsymbol{\Phi}_m(\boldsymbol{\theta})\boldsymbol{\Phi}_n\pi(\boldsymbol{\theta})\mathrm{d}\boldsymbol{\theta} = \gamma_m\delta_{mn},\end{aligned} \tag{6}$$

where $\pi(\boldsymbol{\theta})$ is the joint probability distribution of the reference random variables $\boldsymbol{\Theta}$, δ_{mn} is the Kronecker delta, and γ_m is the squared norm of the polynomials, that is

$$\gamma_m = \mathbb{E}[\boldsymbol{\Phi}_m(\boldsymbol{\theta})\boldsymbol{\Phi}_m(\boldsymbol{\theta})] = 0.5^5 \int_{[-1,1]^5} \boldsymbol{\Phi}_m(\boldsymbol{\theta})\boldsymbol{\Phi}_m(\boldsymbol{\theta})\pi(\boldsymbol{\theta})\mathrm{d}\boldsymbol{\theta}. \tag{7}$$

Depending on the type of distributions of random variables Θ_i, different families of orthogonal polynomials are used. In this case, the Legendre polynomials are used as they are orthogonal with respect to the underlying probability measure defined by the uniformly distributed π_{Θ}.

The coefficients $\boldsymbol{\upsilon}_m$ of the gPC expansion from (3) can be computed by different techniques, e.g. interpolation, orthogonal projection, regression (see e.g. [56]). In this case, coefficients were computed by regression using $Q = 10{,}000$ quasi-Monte Carlo (QMC) sample points generated by the Halton sequence drawn from the uniform distribution $\pi(\boldsymbol{\theta})$. The sample points $\{\boldsymbol{\theta}_j\}_{j=1}^{Q}$ were mapped to parameter vector $\boldsymbol{p}$ for the computation of natural frequencies $\boldsymbol{f}$ according to (2). Their ordering was defined according to the MAC criterion, using the mode shapes of the initial model as a reference. In contrast to the previous research [42], mode shapes were easily clustered only by MAC value for the majority of the sample points. Out of 10,000 sample points $\boldsymbol{\theta}_j$, 9 were filtered out for not being able to connect the 4th mode, which presumably switched order with the 5th mode and was therefore not saved. The mode shapes of the remaining $\widetilde{Q} = 9{,}991$ sample points were well distinguished with MAC values above 0.92 for the correlated modes and MAC values below 0.41 for the uncorrelated modes. To compute the coefficients, the error of the approximation $\boldsymbol{f}_{\text{gPC}}(\boldsymbol{\theta}_j)$ at a sample point $\boldsymbol{\theta}_j$ is defined as

$$\boldsymbol{e}(\boldsymbol{\theta}_j) = \boldsymbol{f}(\boldsymbol{\theta}_j) - \boldsymbol{f}_{\text{gPC}}(\boldsymbol{\theta}_j) = \boldsymbol{f}(\boldsymbol{\theta}_j) - \sum_{m=1}^{M} \boldsymbol{\upsilon}_m\boldsymbol{\Phi}_m(\boldsymbol{\theta}_j). \tag{8}$$

By regression, the coefficients are computed such that the mean squared error of the approximation at the chosen sample points

$$s_k = \sum_{j=1}^{\widetilde{Q}} ([\boldsymbol{e}(\boldsymbol{\theta}_j)]_k)^2 \tag{9}$$

is minimised independently for each of the $k = 1, \ldots, 4$ natural frequency.

To select the degree of polynomials $\boldsymbol{\Phi}_m(\boldsymbol{\theta})$, cross-validation was performed. One of the techniques for validation of the surrogate model is a repeated random sub-sampling validation, where the set of $\widetilde{Q}$ sample points is randomly divided between the training set and the validation set. The training set – 90 % of the sample points – is used to fit a surrogate model and the validation set with V sample points – the remaining 10 % of the sample points – is used to estimate the error. The procedure is repeated with 10 random splits. The relative error of the gPC approximation in the jth validation point $\boldsymbol{\theta}_V^{(r,j)}$ of the rth split was estimated by

$$\epsilon_{\text{rel},k}^{(r,j)} = \frac{|\hat{f}_k^{rt}(\boldsymbol{\theta}_V^{(r,j)}) - f_k(\boldsymbol{\theta}_V^{(r,j)})|}{|f_k(\boldsymbol{\theta}_V^{(r,j)})|}, \tag{10}$$

where f_k denotes the kth eigenfrequency computed by the FE model and $\hat{f}_k^{rt}$ is its gPC approximation of maximum total degree t computed from the training points of the rth split. The mean relative error $\epsilon_{\text{rel},k}$ that is averaged over all the validation points of the 10 splits is shown in Fig. 8.

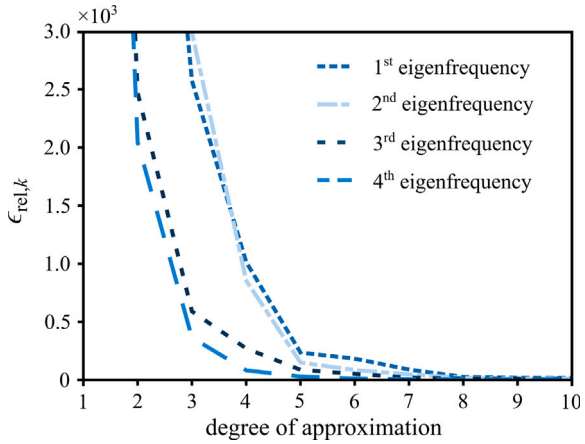

Fig. 8. Cross-validation of the surrogate model.

The curves of relative errors flatten at around 8th degree of approximation and due to the limited number of QMC sample points start to increase at around 10th degree, therefore, the 8th degree is taken for the final surrogate model. The average relative error for all 4 eigenfrequencies is lower than 10^{-4}, while none of the validation points exceeds the relative error of 10^{-3}.

Global sensitivity analysis can also be inexpensively performed to find the influence of varying the input parameters (individually or their combination) on the variance of the quantity of interest. The Sobol' indices are normally computed by Monte Carlo simulation, but with the available gPC surrogate model, they can be computed analytically [57]. The main contribution comes from first-order sensitivity indices as shown in Fig. 9. Smaller contributors and higher-order indices are merged together under the label "other". It can be observed that different modes are quite uniquely influenced by different parameters. Generally, the uncertainty of the in-plane shear modulus of the walls (parameters P_2 and P_3) contributes the most to the variance of the natural frequencies. The vertical stiffness of the foundation (P_4) is very influential in the first two modes (bending in weaker and stronger directions). It should be noted that a large initial uncertainty was assumed. The uncertainty of parameter P_1 that simulates the effect of perpendicular-to-the-grain slab deformations under the CLT walls is moderately influential. Its largest contribution is observed in the first natural frequency. Finally, the uncertainty of the total building mass contributes to approximately a quarter of the variance of the natural frequencies. It should be noted that such a large contribution is attributed to the poor available documentation about the mass of certain elements as discussed in Section 2 and Table 5.

5. Bayesian model updating

Bayesian inference allows for the possibility of updating the initial model while taking into account the uncertainties associated with the lack of knowledge about the model and the error of the experiments. In contrast to the classical deterministic model updating, it provides an estimate of confidence in the results through a probability distribution of updated parameters. A theoretical background of the probabilistic framework for model updating is presented in Section 5.1. The results are presented in Section 5.2 and discussed in Section 5.3.

5.1. Framework

With a probabilistic identification, a conditional distribution of the input random variables $\boldsymbol{\theta}$ given a specific measured value $\boldsymbol{f}_{\text{meas}}$ of the measurable quantity $\boldsymbol{f}$ is sought. The updated, posterior distribution of the parameters according to Bayes' theorem is

$$\pi(\boldsymbol{\theta}|\boldsymbol{f}_{\text{meas}}) = \frac{\pi(\boldsymbol{f}_{\text{meas}}|\boldsymbol{\theta})\pi(\boldsymbol{\theta})}{\int_{\Gamma_\theta} \pi(\boldsymbol{f}_{\text{meas}}|\boldsymbol{\theta})\pi(\boldsymbol{\theta})d\boldsymbol{\theta}} = \frac{\mathcal{L}(\boldsymbol{\theta})\pi(\boldsymbol{\theta})}{\zeta}, \tag{11}$$

where the numerator is the product of the likelihood and the prior and the denominator – the evidence – is just the normalisation factor assuring that the density function integrates to one. The likelihood $\mathcal{L}(\boldsymbol{\theta}) = \pi(\boldsymbol{f}_{\text{meas}}|\boldsymbol{\theta})$ of measuring a specific value of $\boldsymbol{f}_{\text{meas}}$ given the parameters $\boldsymbol{\theta}$ is defined by the probability of the error $\boldsymbol{\epsilon} = \boldsymbol{f}_{\text{meas}} - \boldsymbol{f}_{\text{gPC}}$, where the measured natural frequencies are mean values identified by analysing the 9 min intervals (see Table 1). The error $\boldsymbol{\epsilon}$ includes errors of the modelling and the measurements. It is assumed to be normally distributed, i.e. $\boldsymbol{E} \sim \mathcal{N}(\boldsymbol{0}, \boldsymbol{\Sigma})$, with mutually independent components. Hence, the covariance matrix $\boldsymbol{\Sigma}$ is diagonal with elements $\Sigma_{kk} = \sigma^2_{\boldsymbol{E},k}$. Those are calculated using standard deviations of experimentally identified natural frequencies listed in Tale 1. The likelihood is assumed to be

$$\mathcal{L}(\boldsymbol{\theta}) = 2\pi^{-2}\det(\boldsymbol{\Sigma})^{-\frac{1}{2}} e^{-\frac{1}{2}(\boldsymbol{f}_{\text{meas}} - \mathcal{M}_{\text{gPC}}(\boldsymbol{\theta}))^T \boldsymbol{\Sigma}^{-1}(\boldsymbol{f}_{\text{meas}} - \mathcal{M}_{\text{gPC}}(\boldsymbol{\theta}))}. \tag{12}$$

The prior $\pi(\boldsymbol{\theta})$ is assumed to be uniformly distributed as was defined in (5).

5.2. Results

With likelihood and prior defined according to (5) and (12), respectively, posterior distribution was sampled using Metropolis–Hastings algorithm. Altogether, 100 simultaneous random walks were initiated. After the burn-in period of 1,500 steps, each random walk consisted of 10,000 steps. A total of 1,000,000 sample points were acquired and analysed in Fig. 10. In diagonal plots, the histograms and the kernel density estimations (KDE) of the posterior probability distributions are shown. Pairwise comparisons are shown in off-diagonal scatter plots to identify possible interactions between the parameters. A positive correlation can be observed between P_2 and P_5, and between P_1 and P_5. This is an obvious interaction between stiffness parameters (P_1 and P_2) and mass parameter P_5, from which it can be deduced that reducing the uncertainty of mass of the building would result in lower variability of parameters P_1 and P_2 and thus more reliable conclusions. The model updating results would benefit greatly from reducing the uncertainty of the mass, which emanates from the lack of available documentation.

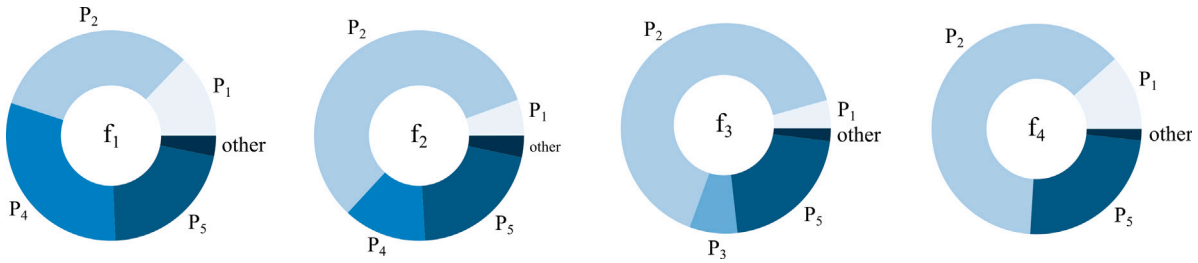

Fig. 9. Sobol' indices of the input parameters: coefficient of vertical stiffness of the walls (P_1), coefficient of the in-plane shear stiffness of the walls (P_2), coefficient of the in-plane shear stiffness of the external walls (P_3), the stiffness of the springs modelling the foundation (P_4), and coefficient of the total mass of the building (P_5). Smaller first-order and higher-order contributors are merged under the label "other".

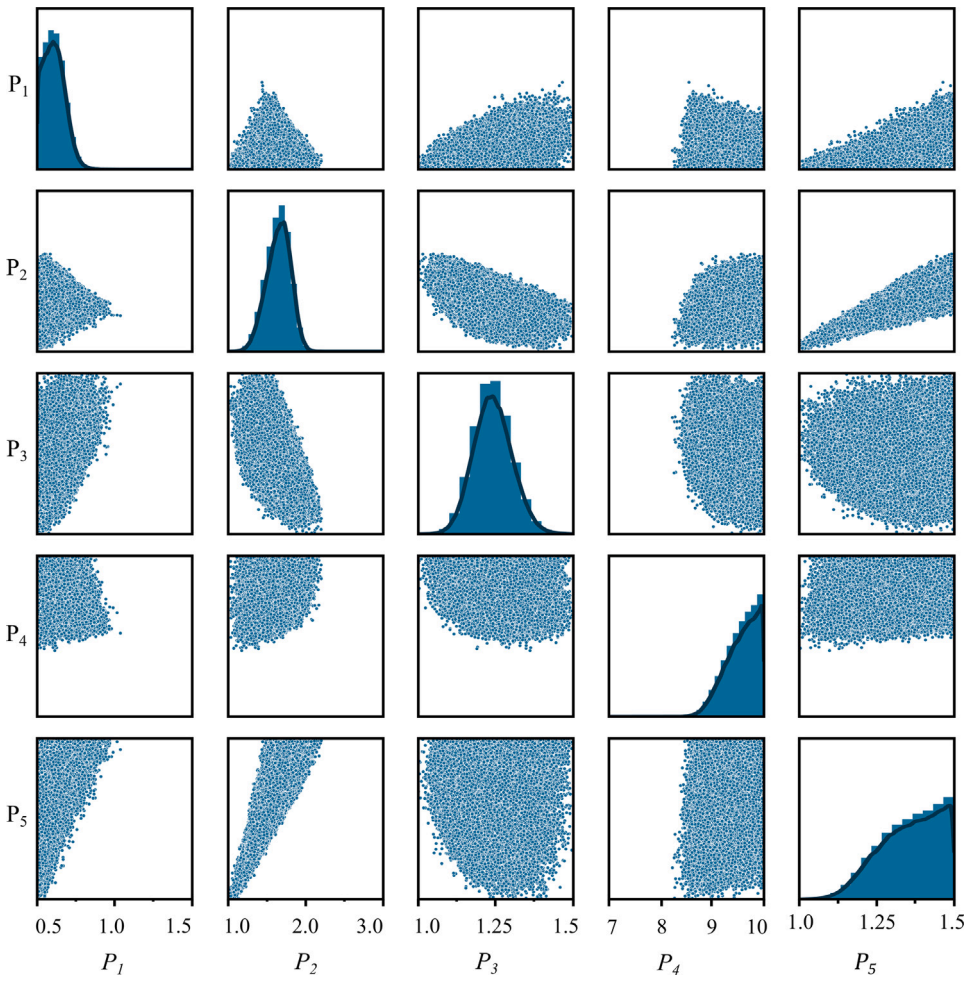

Fig. 10. Pairwise scatter plots of posterior distribution sampled with MCMC are shown in off-diagonal plots. Diagonal plots show histograms of the parameter occurrences and KDE of the posterior distribution for parameters: coefficient of vertical stiffness of the walls (P_1), coefficient of the in-plane shear stiffness of the walls (P_2), coefficient of the in-plane shear stiffness of the external walls (P_3), the stiffness of the springs modelling the foundation (P_4), and coefficient of the total mass of the building (P_5).

Another correlation – this time negative – can be observed between P_2 and P_3. Both are factors contributing to the shear modulus of the walls — P_2 of all the walls and P_3 only of the external walls. A lower value of one parameter implies a higher value of the other. Such definition of the parameters was selected due to computation convenience, but a better presentation of the results is possible by defining in-plane shear modulus of internal walls $G_{\text{walls,in}} = P_2 \cdot G_{12}$ as one derived parameter and external walls $G_{\text{walls,ex}} = P_2 \cdot P_3 \cdot G_{12}$ as the other. Distributions of those two derived parameters and a scatter plot are shown in Fig. 11.

The presented results are based on the Bayesian updating using four natural frequencies in the likelihood, however, three additional iterations were performed to observe the progression of the results due to adding each of the four modes to the likelihood. Besides changing the number of the natural frequencies in (2), the updating procedure remained the same. Initially, only the first natural frequency was used in the likelihood. Then, the second and the third modes were added, and finally, Bayesian updating was performed with all four modes included. The KDEs of posterior parameter distributions from the four iterations of Bayesian updating are shown in Fig. 12.

A significant improvement in the reduced posterior uncertainty can be observed when the fourth mode is added, mainly in parameters P_1 and P_4. The two parameters both influence the vertical stiffness — P_1 is connected to the elastic modulus of vertical CLT wall layers and P_4 to the vertical foundation stiffness. When the first three modes are included in the updating, a negative interaction between the two parameters can be observed (see Fig. 13). A wide range of values is allowed for both parameters. By including the fourth mode in the updating, the effects of those two parameters are better distinguished.

The uncertainty quantification of the initial model (prior knowledge of parameters) and the updated model (posterior distribution) is shown in Fig. 14.

5.3. Discussion

Several observations can be made from the results of the updating. First, the posterior distribution of parameter P_1 suggests a reduction of stiffness of vertical layers to 50 %–75 % of the initial value. This goes in line with previous research [36], where a similar reduction was observed. The justification for such a significant drop in stiffness is the perpendicular-to-the-grain deformation of floor slabs under the walls. This applies only to the platform-frame buildings. A more detailed explanation of the effect is presented in [36].

Secondly, the in-plane shear modulus of CLT panels is observed to be most likely between 300 MPa and 500 MPa for the internal walls and about 20 % higher for the external walls. In-plane shear modulus of CLT is fairly uncertain material property, with expected values ranging between 250 MPa, which was provided by ETA [52], and 450 MPa to 650 MPa, which was suggested by [55] for CLT panels without or with narrow sides glued together, respectively. But this value, even though it is implemented as a material property of CLT, involves more effects. It takes into account also the contribution of the non-structural elements

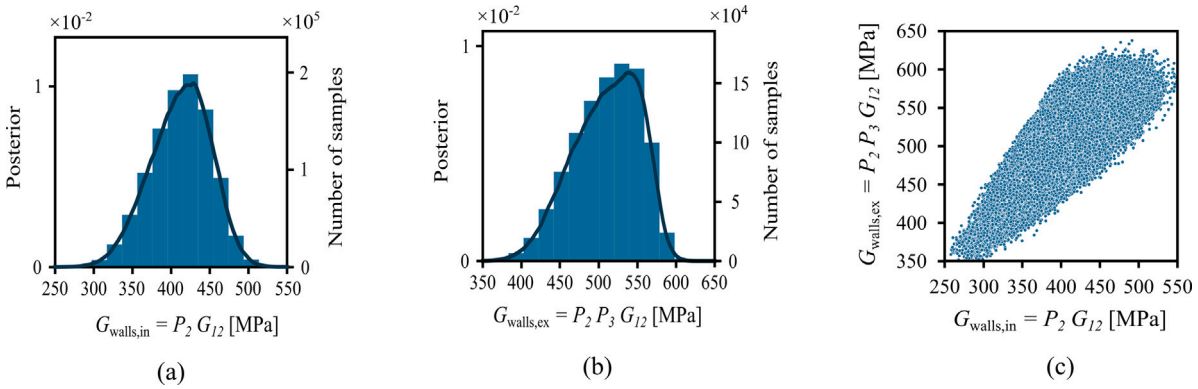

Fig. 11. Posterior distribution of the in-plane shear modulus of (a) the internal walls $G_{walls,in}$, (b) external walls $G_{walls,ex}$, and (c) a scatter plot of samples projected in the 2D parameter plane ($G_{walls,in}$ and $G_{walls,ex}$). In plots (a) and (b) a histogram is shown together with a KDE of the posterior distribution.

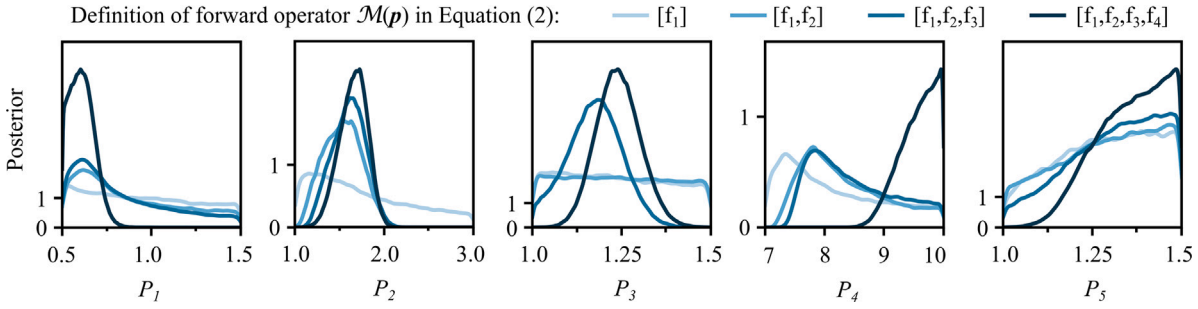

Fig. 12. KDEs of posterior parameter distributions when different sets of modes are included in the Bayesian updating.

(such as plasterboards and façade) or possible reduction of the stiffness due to steel connections. With all those uncertainties, it may not be possible to precisely pinpoint which effects and to what extent are responsible for the updated value. However, due to the very simplistic design of the building (thin cladding of the façade and many exposed internal walls), the updated values are within a reasonable range.

Lastly, the vertical stiffness of the foundation is observed to be higher than 10^9 N/m/m^2. Considering the one-at-a-time sensitivity of this parameter using the updated values of the other parameters (see Fig. 15), the updated value suggests an almost fully constrained boundary condition. Increasing the stiffness does not increase the natural frequency any more.

Mass parameter P_5 was included in the updating to account for its uncertainty and not as much for learning about the actual mass. By including it, the distributions of other stiffness parameters (especially P_2 and P_3) were wider and thus reflected a more realistic estimation of confidence in the results. An important remark is that by reducing the uncertainty of the mass of the building (which was not possible due to unavailable documentation), the updating would result in narrower posterior distributions of stiffness parameters leading to more reliable conclusions. One should always strive to reduce such uncertainty when performing model updating. Another possibility for improving the reliability of the results is by obtaining more measurements. The study has clearly shown an improvement of the results from adding more modes of vibration to the likelihood function.

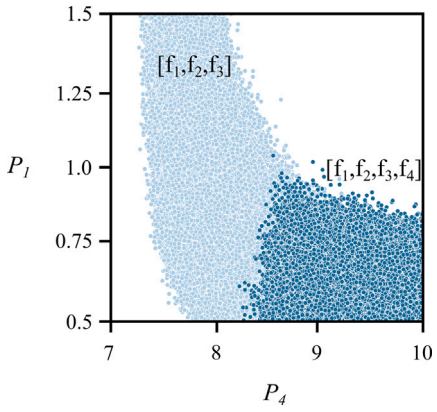

Fig. 13. A scatter plot of posterior samples in P_1–P_4 parameter plane for iterations with 3 and 4 modes included.

6. Conclusion

An eight-storey CLT building, located in Ås, Norway, was analysed by AVT, obtaining four modes of vibration. A detailed FE model of the building was assembled to compute its modal properties. The initial model underestimated natural frequencies by up to 15 % (perhaps due to the in-plane shear modulus provided by ETA being very low).

A parametric study on the modelling of geometry and mass distribution was performed. With different assumptions of simplifying geometry (such as removing parapets and lintels, or filling the openings), modal properties were significantly altered. Therefore, when considering similar timber buildings, it is suggested that the geometry is precisely modelled. An accurate estimation of the building's mass is also important, while its distribution over each storey can be smeared. However, it needs to be emphasised that no substantial mass imbalances were present in the design of this building.

The model was updated with a surrogate-based Bayesian inference using the measurements of all 4 modes of vibration. Several case-specific conclusions were drawn:

- The vertical stiffness of the building is significantly lower than initially anticipated, most likely due to the effect of perpendicular-to-the-grain deformations of CLT floor slabs under the walls.

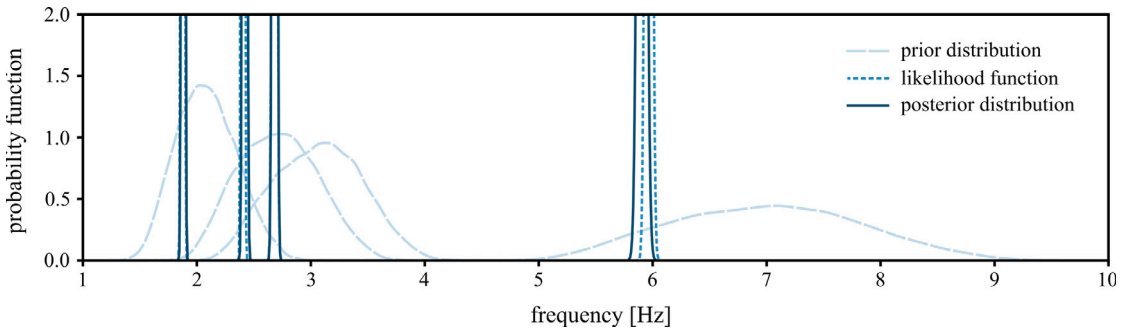

Fig. 14. Prior, posterior and measured frequencies.

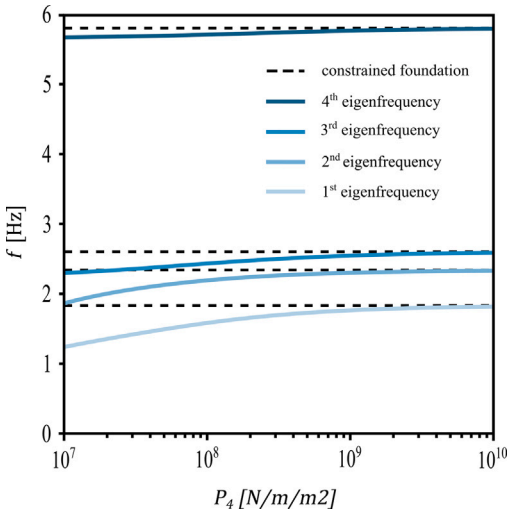

Fig. 15. One-at-a-time sensitivity analysis for parameter P_4 while other parameters are set to the updated values. Natural frequencies are asymptotically approaching those of the model with constrained foundations.

- The value of the in-plane shear modulus of CLT panels is very uncertain. The updated value of the shear modulus of CLT panels is most likely between 300 MPa and 500 MPa for internal walls and about 20 % higher for external walls. However, in addition to the already uncertain in-plane shear modulus, the value includes various other effects, such as non-structural elements, steel connections, and possible cracks in the panels. Therefore, it is not possible to pinpoint the responsible contributors.
- The foundation was found to be stiff. A constrained boundary condition of the ground floor is a suitable assumption in the observed case.

Those conclusions should not be directly replicated when modelling other buildings, nevertheless, there is a potential for generalisation after the set of similar case studies is expanded.

The model updating was repeated in three iterations while changing the number of modes that are included in the likelihood. The results showed a significant improvement from increasing the number of modes (especially after adding the fourth mode). In future attempts to perform model updating when the aim is to identify modelling parameters, an emphasis should be put on maximising the amount of obtained experimental data. Another potential for improving the reliability of the results (and thus achieving more precisely identified parameters) is seen in reducing the uncertainty of the building's mass.

CRediT authorship contribution statement

Blaž Kurent: Writing – original draft, Visualization, Methodology, Investigation, Conceptualization. **Noemi Friedman:** Writing – original draft, Methodology, Conceptualization. **Angelo Aloisio:** Writing – original draft, Conceptualization. **Dag Pasca:** Writing – original draft, Investigation. **Roberto Tomasi:** Supervision, Project administration. **Boštjan Brank:** Writing – review & editing, Supervision, Project administration, Conceptualization.

Declaration of competing interest

The authors declare that they have no known competing financial interests or personal relationships that could have appeared to influence the work reported in this paper.

Data availability

Data will be made available on request.

Acknowledgements

The financial support of Slovenian Research Agency for BK and BB is gratefully acknowledged (J2-2490). Hungarian Ministry of Innovation and Technology NRDI Office within the framework of the Artificial Intelligence National Laboratory Program and the Hungarian National Research, Development and Innovation Office is also acknowledged for the support (SNN 134368). This work has been also partially funded by the BUILDCHAIN project (https://buildchain-project.eu/). BUILDCHAIN has received funding from the EU's Horizon Europe research and innovation program under grant agreement 101092052.

References

[1] A. Aloisio, D.P. Pasca, Y. De Santis, T. Hillberger, P.F. Giordano, M.M. Rosso, R. Tomasi, M.P. Limongelli, C. Bedon, Vibration issues in timber structures: A state-of-the-art review, J. Build. Eng. (2023) 107098.

[2] R. Abrahamsen, M.A. Bjertnaes, J. Bouillot, B. Brank, L. Cabaton, R. Crocetti, O. Flamand, F. Garains, I. Gavric, O. Germain, et al., Dynamic response of tall timber buildings under service load: The dynaTTB research program, in: EURODYN 2020, XI International Conference on Structural Dynamics, Athens, Greece, 22–24 June 2020, National Technical University of Athens, 2020, pp. 4900–4910.

[3] B.R. Ellis, A.J. Bougard, Dynamic testing and stiffness evaluation of a six-storey timber framed building during construction, Eng. Struct. 23 (10) (2001) 1232–1242.

[4] A. Feldmann, H. Huang, W. Chang, R. Harris, P. Dietsch, M. Gräfe, C. Hein, Dynamic properties of tall timber structures under wind-induced vibration, in: World Conference on Timber Engineering, WCTE 2016, 2016.

[5] T. Reynolds, R. Harris, W.S. Chan, Dynamic response of tall timber buildings to wind load, in: 35th Annual Symposium of IABSE/52nd Annual Symposium of IASS/6th International Conference on Space Structures, London, 2011.

[6] R. Verhaegh, M. Vola, J.D. Jong, Haut - A 21-storey Tall Timber Residential Building, Int. J. High-Rise Build. 9 (3) (2020) 213–220.

[7] M.A. Bezabeh, G.T. Bitsuamlak, M. Popovski, S. Tesfamariam, Dynamic response of tall mass-timber buildings to wind excitation, J. Struct. Eng. (United States) 146 (10) (2020).

[8] I. Mugabo, A.R. Barbosa, M. Riggio, Dynamic characterization and vibration analysis of a four-story mass timber building, Front. Built Environ. 5 (2019).

[9] G. Hafeez, G. Doudak, G. McClure, Effect of nonstructural components on the dynamic characteristics of light-frame wood buildings, Can. J. Civil Eng. 47 (3) (2020) 257–271.

[10] G. Hafeez, G. Doudak, G. McClure, Dynamic characteristics of light-frame wood buildings, Can. J. Civil Eng. 46 (1) (2019) 1–12.

[11] Y.M. Kim, Y.M. Kim, H.J. Kim, T.U. Ha, E.M. Shin, W.J. Kim, Analysis of roof load and dynamic characteristics of traditional timber building considering column axial force and ambient vibration measurement, J. Archit. Inst. Korea 37 (11) (2021) 271–280.

[12] A. Talja, L. Fülöp, Evaluation of Wind-Induced Vibrations of Modular Buildings, VTT Technical Research Centre of Finland, 2016.

[13] I. Mugabo, A.R. Barbosa, A. Sinha, C. Higgins, M. Riggio, S. Pei, J.W. van de Lindt, J.W. Berman, System identification of UCSD-NHERI shake-table test of two-story structure with cross-laminated timber rocking walls, J. Struct. Eng. 147 (4) (2021) 04021018.

[14] F. Magalhães, Á. Cunha, E. Caetano, Vibration based structural health monitoring of an arch bridge: From automated OMA to damage detection, Mech. Syst. Signal Process. 28 (2012) 212–228.

[15] S. Pereira, F. Magalhães, Á. Cunha, C. Moutinho, J. Pacheco, Modal identification of concrete dams under natural excitation, J. Civ. Struct. Health Monit. 11 (2) (2021) 465–484.

[16] A. Cigada, A. Caprioli, M. Redaelli, M. Vanali, Vibration testing at Meazza stadium: Reliability of operational modal analysis to health monitoring purposes, J. Perform. Constr. Facil. 22 (4) (2008) 228–237.

[17] R. Alaggio, A. Aloisio, E. Antonacci, R. Cirella, Two-years static and dynamic monitoring of the Santa Maria di Collemaggio basilica, Constr. Build. Mater. 268 (2021) 121069.

[18] C. Amaddeo, M. Dorn, Dynamic characterization of a six-story light-weight timber-frame building, in: 6th International Conference on Structural Health Assessment of Timber Structures, 7-9 September 2022, Prague, 2022, 2022.

[19] T. Reynolds, A. Feldmann, M. Ramage, W. Chang, R. Harris, P. Dietsch, Design parameters for lateral vibration of multi-storey timber buildings, in: International Network on Timber Engineering Research Proceedings, INTER 2016, 2016.

[20] C. Larsson, O. Abdeljaber, M. Dorn, Dynamic evaluation of a nine-storey timber-concrete hybrid building during construction, Eng. Struct. 289 (2023) 116344.

[21] C. Medel-Vera, M.C. Contreras, Resilience-based predictive models for the seismic behaviour of mid-rise, base-isolated CLT buildings for social housing applications in Chile, J. Build. Eng. 44 (2021).

[22] M. Johansson, A. Linderholt, Å. Bolmsvik, K. Jarnerö, J. Olsson, T. Reynolds, Building higher with light-weight timber structures-the effect of wind induced vibrations, in: 44th International Congress and Exposition on Noise Control Engineering, INTER-NOISE 2015, 2015.

[23] M. Johansson, A. Linderholt, K. Jarnerö, P. Landel, Tall timber buildings—A preliminary study of wind-induced vibrations of a 22-storey building, Proc. WCTE (2016).

[24] I. Edskar, H. Lidelow, Wind-induced vibrations in timber buildings-parameter study of cross-laminated timber residential structures, Struct. Eng. Int. 27 (2) (2017) 205–216.

[25] I. Edskär, H. Lidelöw, Dynamic properties of cross-laminated timber and timber truss building systems, Eng. Struct. 186 (2019) 525–535.

[26] X. Zhao, B. Zhang, T. Kilpatrick, I. Sanderson, Numerical analysis on global serviceability behaviours of tall clt buildings to the eurocodes and uk national annexes, Buildings 11 (3) (2021).

[27] X. Zhao, B. Zhang, T. Kilpatrick, I. Sanderson, D. Liu, Numerical analysis on global serviceability behaviours of tall glulam frame buildings to the eurocodes and UK national annexes, J. Civ. Eng. Construct. 10 (3) (2021) 109–122.

[28] P. Landel, M. Johansson, A. Linderholt, Comparative study of wind-induced accelerations in tall timber buildings according to four methods, in: WCTE 2021, World Conference on Timber Engineering, Santiago, Chile, 9-12 August, 2021.

[29] A.S. Cao, H. Stamatopoulos, A theoretical study of the dynamic response of planar timber frames with semi-rigid moment-resisting connections subjected to wind loads, Eng. Struct. 240 (2021).

[30] E. Lazzarini, G. Frison, D. Trutalli, L. Marchi, R. Scotta, Comfort assessment of high-rise timber buildings exposed to wind-induced vibrations, Struct. Des. Tall Special Build. 30 (12) (2021).

[31] A.C. Altunisik, O.S. Karahasan, F.Y. Okur, E. Kalkan, K. Ozgan, Finite Element Model Updating and Dynamic Analysis of a Restored Historical Timber Mosque Based on Ambient Vibration Tests, ASTM International, 2019.

[32] A.C. Altunişik, O.Ş. Karahasan, F.Y. Okur, E. Kalkan, K. Özgan, Ambient vibration test and modelling of historical timber mosques after restoration, Proc. Inst. Civ. Eng. 173 (12) (2020) 956–968.

[33] N.F. Alkayem, M. Cao, Y. Zhang, M. Bayat, Z. Su, Structural damage detection using finite element model updating with evolutionary algorithms: a survey, Neural Comput. Appl. 30 (2) (2018) 389–411.

[34] A. Teughels, J. Maeck, G. De Roeck, Damage assessment by FE model updating using damage functions, Comput. Struct. 80 (25) (2002) 1869–1879.

[35] A. Aloisio, D. Pasca, R. Tomasi, M. Fragiacomo, Dynamic identification and model updating of an eight-storey CLT building, Eng. Struct. 213 (2020) 110593.

[36] B. Kurent, B. Brank, W.K. Ao, Model updating of seven-storey cross-laminated timber building designed on frequency-response-functions-based modal testing, Struct. Infrastruct. Eng. 19 (2) (2023) 178–196.

[37] S. Tulebekova, K.A. Malo, A. Rønnquist, P. Nåvik, Modeling stiffness of connections and non-structural elements for dynamic response of taller glulam timber frame buildings, Eng. Struct. 261 (2022).

[38] S. Tulebekova, K.A. Malo, A. Rønnquist, Dynamic identification and model calibration of connection stiffness in multi-storey cross-laminated timber buildings, J. Build. Eng. 72 (2023) 106607.

[39] James L. Beck, Lambros S. Katafygiotis, et al., Updating models and their uncertainties. I: Bayesian statistical framework, J. Eng. Proc. ASCE 124 (4) (1998) 455–462.

[40] N. Shirzad-Ghaleroudkhani, M. Mahsuli, S.F. Ghahari, E. Taciroglu, Bayesian identification of soil-foundation stiffness of building structures, Struct. Control Health Monit. 25 (3) (2018) e2090.

[41] C. Leyder, E. Chatzi, A. Frangi, Vibration-based model updating of a timber frame structure, Procedia eng. 199 (2017) 2132–2139.

[42] B. Kurent, N. Friedman, W.K. Ao, B. Brank, Bayesian updating of tall timber building model using modal data, Eng. Struct. 266 (2022) 114570.

[43] M.A. Bezabeh, G.T. Bitsuamlak, M. Popovski, S. Tesfamariam, Probabilistic serviceability-performance assessment of tall mass-timber buildings subjected to stochastic wind loads: Part I - structural design and wind tunnel testing, J. Wind Eng. Ind. Aerodyn. 181 (2018) 85–103.

[44] M.A. Bezabeh, G.T. Bitsuamlak, M. Popovski, S. Tesfamariam, Probabilistic serviceability-performance assessment of tall mass-timber buildings subjected to stochastic wind loads: Part II - structural reliability analysis, J. Wind Eng. Ind. Aerodyn. 181 (2018) 112–125.

[45] E. Ussher, C.U.D. Gurholt, J.N. Mikalsen, A. Aloisio, R. Tomasi, Effect of construction features on the dynamic performance of mid-rise CLT platform-type buildings, Wood Mater. Sci. Eng. (2022) 1–13.

[46] B. Kurent, W.K. Ao, A. Pavic, F. Pérez, B. Brank, Modal testing and finite element model updating of full-scale hybrid timber-concrete building, Eng. Struct. 289 (2023) 116250.

[47] W.K. Ao, A. Pavic, B. Kurent, F. Perez, Novel FRF-based fast modal testing of multi-storey CLT building in operation using wirelessly synchronised data loggers, J. Sound Vib. 548 (2023) 117551.

[48] C. Larsson, O. Abdeljaber, Å. Bolmsvik, M. Dorn, Long-term analysis of the environmental effects on the global dynamic properties of a hybrid timber-concrete building, Eng. Struct. 268 (2022).

[49] G. Granello, A. Palermo, Monitoring dynamic properties of a pres-lam structure: trimble navigation office, J. Perform. Constr. Facil. 34 (1) (2020) 04019087.

[50] B. Peeters, G. De Roeck, Reference-based stochastic subspace identification for output-only modal analysis, Mech. Syst. Signal Process. 13 (6) (1999) 855–878.

[51] D.P. Pasca, A. Aloisio, M.M. Rosso, S. Sotiropoulos, PyOMA and PyOMA_GUI: a python module and software for operational modal analysis, SoftwareX 20 (2022) 101216.

[52] Mayr-Melnhof, European Technical Assesment ETA-09/0036 of 15.01.2020, Technical Report, Austrian Institute of Construction Engineering, 2020.

[53] R.J. Allemang, The modal assurance criterion - Twenty years of use and abuse, Sound Vib. 37 (8) (2003) 14–21.

[54] D. Fotsch, D.J. Ewins, Further applications of the FMAC, in: Proceedings of the International Modal Analysis Conference, Vol. 1, IMAC, 2001, pp. 635–639.

[55] R. Brandner, G. Flatscher, A. Ringhofer, G. Schickhofer, A. Thiel, Cross laminated timber (CLT): overview and development, Eur. J. Wood Wood Prod. 74 (3) (2016) 331–351.

[56] Dongbin X., Numerical Methods for Stochastic Computations: A Spectral Method Approach, Princeton University Press, 2010.

[57] B. Sudret, Global sensitivity analysis using polynomial chaos expansions, Reliab. Eng. Syst. Saf. 93 (7) (2008) 964–979.